

Search for neutrino emission from relic dark matter in the Sun with the Baikal NT200 detector

A.D. Avrorin^a, A.V. Avrorin^a, V.M. Aynutdinov^a, R. Bannasch^g, I.A. Belolaptikov^b, D.Yu. Bogorodsky^c, V.B. Brudanin^b, N.M. Budnev^c, I.A. Danilchenko^a, S.V. Demidov^a, G.V. Domogatsky^a, A.A. Doroshenko^a, A.N. Dyachok^c, Zh.-A.M. Dzhilkibaev^a, S.V. Fialkovsky^e, A.R. Gafarov^c, O.N. Gaponenko^a, K.V. Golubkov^a, T.I. Gress^c, Z. Honz^b, K.G. Kebkal^g, O.G. Kebkal^g, K.V. Konischev^b, E.N. Konstantinov^c, A.V. Korobchenko^c, A.P. Koshechkin^a, F.K. Koshel^a, A.V. Kozhin^d, V.F. Kulepov^e, D.A. Kuleshov^a, V.I. Ljashuk^a, M.B. Milenin^e, R.A. Mirgazov^c, E.R. Osipova^d, A.I. Panfilov^a, L.V. Pan'kov^c, A.A. Perevalov^c, E.N. Pliskovsky^b, V.A. Poleschuk^c, M.I. Rozanov^f, V.F. Rubtzov^c, E.V. Rjabov^c, B.A. Shaybonov^b, A.A. Shefler^a, A.V. Shkurihin^d, A.A. Smagina^b, O.V. Suvorova^{a,*}, B.A. Tarashansky^c, S.A. Yakovlev^g, A.V. Zagorodnikov^c, V.A. Zhukov^a, V.L. Zurbanov^c

^a*Institute for Nuclear Research, 60th October Anniversary pr. 7A, Moscow 117312, Russia*

^b*Joint Institute for Nuclear Research, Dubna 141980, Russia*

^c*Irkutsk State University, Irkutsk 664003, Russia*

^d*Skobeltsyn Institute of Nuclear Physics MSU, Moscow 119991, Russia*

^e*Nizhni Novgorod State Technical University, Nizhni Novgorod 603950, Russia*

^f*St. Petersburg State Marine University, St. Petersburg 190008, Russia*

^g*EvoLogics GmbH, Berlin, Germany*

Abstract

We have analyzed a data set taken over 2.76 years live time with the Baikal neutrino telescope NT200. The goal of the analysis is to search for neutrinos from dark matter annihilation in the center of the Sun. Apart from the conventional annihilation channels $b\bar{b}$, W^+W^- and $\tau^+\tau^-$ we consider also the annihilation of dark matter particles into monochromatic neutrinos. From the absence of any excess of events from the direction of the Sun over the expected background, we derive 90% upper limits on the fluxes of muons and muon neutrinos from the Sun, as well as on the elastic cross sections of dark matter scattering on protons.

Keywords:

1. Introduction

According to numerous astronomical and cosmological observations, there exists a non-luminous form of matter which is responsible for about 90% of the mass within galaxies and clusters of galaxies. Results from cosmic microwave background measurements by both space- and ground-based experiments (e.g., [1], [2], [3], [4]) are remarkably consistent with the predictions of the standard cosmological model in which the constituents of a spatially-flat and expanding Universe are dominated by cold dark matter (CDM) and a cosmological constant (Λ) at later times (Λ CDM model). Moreover, recent direct observations of several merging clusters support a collisionless dark matter scenario [5]. New collisionless dark matter (DM) particles can naturally appear in models beyond the Standard Model (SM). Supposed to be massive DM particles could be captured by astrophysical bodies (including the Sun) and accumulate inside them over cosmological times. The most interesting range of DM particle masses for this scenario – from a few GeV to hundreds of TeV – naturally arises in many classes of theoretical models. Among the possible

*Corresponding author

Email address: suvorova@cpc.inr.ac.ru (O.V. Suvorova)

candidates for CDM of this kind of particles are the lightest superpartners in supersymmetric models [6], Kaluza-Klein particles in models with extra dimensions [7] or 4th generation heavy neutrinos [8]. Through self-interactions, DM pairs could annihilate into ordinary particles, and among the final products of these annihilations could be high energy neutrinos [9]. Those are able to reach the Earth and could be observed over the background of atmospheric neutrinos. High energy neutrino telescopes (NTs [10]) like the present and future deep underwater detectors in Lake Baikal [11, 12] can identify possible sources of clumped dark matter if they observe a significant excess in the number of neutrino events from the direction of the dark matter accumulation.

In this paper we analyse neutrino-induced upward going muons which have been measured with the Baikal neutrino telescope NT200 between April 1998 and February 2003. We study correlations of the arrival directions with the Sun annual path. Some preliminary results can be found in Ref. [13]. Here we perform a completely new analysis of those data. We consider several possible annihilation channels, assuming a 100% branching ratio for each channel as extreme cases. The annihilation channels differ by the neutrino energy spectra and their flavour content produced from generated particles decays. Soft spectra are dominated by energies much smaller than the mass of the DM particles and emerge e.g. from $b\bar{b}$ decays, hard spectra emerge from decays into $\tau^+\tau^-$ or W^+W^- pairs. To fully acknowledge flavour content of neutrino spectra we also consider the annihilation of dark matter into monochromatic neutrinos of all possible flavours. Another reason why we pay attention to monochromatic neutrinos is that they represent examples of the most energetic neutrino emissions in DM annihilations (we also refer reader to the analysis of monochromatic neutrino signal in NTs performed in Refs. [14, 15]). We numerically optimized the sizes of the half cones toward the Sun in dependence on to the assumed mass of the DM particle. Finally, we compare our results with other experiments looking for neutrino signal from DM annihilations in the Sun as well as with the results of direct searches (for review see e.g. [16]).

2. Experiment and data selection

The neutrino telescope NT200 was completed in 1998. It is one of several deep underwater installations operating now in the southern basin of Lake Baikal, at a distance of 3.5 km off the shore and at a depth of 1.1 km. Its goals are the study of high energy muons and neutrinos coming from the top and bottom hemispheres, respectively. The NT200 configuration and its main functional systems have been described in details elsewhere [17, 18]. The detector consists of 192 optical modules arranged pair-wise on 8 strings of 72 m length: seven peripheral strings and a central one. The distances between the strings are about 20 m. Each OM contains hybrid photodetector QUASAR-370, a photo multiplier tube (PMT) with 37-cm diameter. To suppress background from bioluminescence and dark noise, the two PMTs of a pair are switched in coincidence within a time window of 15 ns. Since 2005, the NT200 configuration has been upgraded by additional 3 strings each 100 m away from the centre. This upgraded detector, named NT200+, served as a prototype cell on the 10 Mton scale for a future Gigaton volume detector [12] whose first cluster of 5 strings is operating since February 2014 [19].

Relativistic particles crossing the effective volume of a deep underwater telescope are detected via their Cherenkov radiation. This radiation is recorded by optical modules (OMs) which are time-synchronized and energy-calibrated by artificial light pulses. At 1 km depth, the muon flux from cosmic ray interactions in the upper hemisphere is about one million times higher than the flux of upward going muons initiated by neutrino interactions in water and rock below the array. Our analysis is based on data selection and event reconstruction described in details previously, as in Ref. [11, 20]. We recall them here briefly. The muon trigger requires $N_{hit} \geq n$ within 500 ns, where hit refers to a pair of OMs coupled in a channel and n is set to 3 or 4. The first cut level selects events with at least 6 hits on at least 3 strings ("6/3"), retaining about 40% of all triggered events. Given the huge ratio of downward to upward moving muons, the selection of a clean sample of true upward muons is a major challenge and requires a highly efficient rejection of misreconstructed downward moving muons. Therefore, a number of quality cuts is applied during off-line data processing [11, 20]. Most fake events (downward muons mis-reconstructed as upward muons) are due to muon bundles and populate directions close to the horizon. Therefore only events with zenith angles larger than 100° were selected. The average rate of such events was 0.037 Hz. Further optimization of the data

selection criteria was performed using simulated neutrino events [20] with a spectrum following [21], as well as events from downward going atmospheric muons generated with the help of CORSIKA [22] and propagated with the MUM code [23]. To get the best possible estimator in reconstruction of a muon trajectory, multiple start guesses for the χ^2 minimization are used:

$$\chi^2 = \frac{1}{(N_{hit} - 5)} \sum_{i=1}^{N_{hit}} \frac{(T_i(\theta, \phi, u_0, v_0, t_0) - t_i)^2}{\sigma_{ti}^2}. \quad (1)$$

Here, t_i are the measured times and T_i are the times expected for a given track hypothesis, σ_{ti} are the timing errors. A set of parameters defining a track hypothesis is given by θ and ϕ – the zenith and azimuth angle of the track, respectively, u_0 and v_0 – the two coordinates of the track point closest to the centre of the detector, and t_0 – the time the muon passes this point. The next step is the application of quality cuts to variables like the number of hit channels, the probabilities of fired channels to have been hit or not; the actual position of the track with respect to the detector centre; the minimal residual between expected and detected times for hit channels; the smoothness of the channel response probabilities along the reconstructed track and $\chi^2/\text{d.o.f.}$ [20]. These selection criteria were designed and optimized for the separation of atmospheric neutrinos from the background of fake events from atmospheric muons. They provide a rejection factor for atmospheric muons of about 10^{-7} , resulting in a neutrino energy threshold of about 10 GeV and a mean value 4.3° for the distribution of mismatch angles (compared to 14.1° after the initial “6/3” selection). The r.m.s. angle is 4.7° and the median value 2.5° . Note that in the further search for the optimal size of the signal cones towards the Sun direction we use the shape of the angular distribution itself.

The NT200 coordinates are 51.83°N and 104.33°E . The skyplot of the final sample of neutrino events in equatorial coordinates is shown in Fig 1. The colour gradient marks the sky visibility for NT200, the line follows the track of the Sun averaged over a year. The total number of selected events surviving all cuts [13], [20] is 510, for 1038 days of live time. We use a re-sampling (bootstrap) method to get the background by random mixing of arrival directions and times from the selected data sample. In Fig 2 we show the numbers of observed events (red histogram with points) and background (blue triangles) as a function of the angle between the Sun direction and the muon track. The blue line is a fit to the background. We do not observe an excess of events from the direction of the Sun. Assuming Poisson statistics, the upper limits on the number of signal events in excess of atmospheric neutrinos have been obtained at 90% confidence level (CL) applying the standard TRolke class in the ROOT analysis package [24]. We leave the discussion of systematic uncertainties for Section 3. Next, based on this result, we derive other limits on parameters which can be easily compared with other experiments or with theoretical predictions.

For the search for signal events from the decay of annihilating DM particles in the Sun we optimize the sizes of cones toward the Sun in a way which gives the best signal-to-background ratio, taking into account for each decay mode the spectrum for signal neutrinos coming at night. For the calculation of the neutrino effective area $A_{eff,\nu}$, we apply the NT200 response function (efficiency) for crossing muons generated in charged current neutrino interactions. We have used the same MC mass production of neutrinos (antineutrinos) as in Ref. [20] and reconstructed muons for twelve NT200 configurations operated in 1998-2003. The following expression describes these calculations:

$$A_{eff,\nu}^i(E_{th}, E_\nu) = V_{MC}^i \times N_A \times \rho \times \sigma^{CC}(E_\nu) \times \epsilon_\nu^i(E_{th}, E_\nu), \quad (2)$$

where $i = 1, \dots, 12$ and ϵ_ν^i is the efficiency of muon reconstruction i.e. the ratio of two-dimensional angular-energy distributions of reconstructed events to simulated neutrinos. The MC weights of each event were included and the Sun trajectory also. The mean value of the generated volumes V_{MC}^i from all twelve configurations is $V_{MC} = 4.406 \times 10^{14} \text{cm}^3$. The product of $N_A \cdot \rho \cdot \sigma^{CC}(E_\nu)$ in (2) is the inverse value of the length of neutrino-nucleon interactions in the Earth. The value N_A is the Avogadro number, ρ the medium density (rock or water), σ^{CC} the neutrino-nucleon cross section in charged current (CC) interactions. The shadowing effect due to the exponential attenuation of the neutrino flux in the Earth is negligible or weak for energies less than 10 TeV and we can omit it in formula (2). The result for the neutrino effective area in dependence on the neutrino energy is shown in Fig. 3 as a black line and labeled ”total”. The convolution of

the effective area A_{eff}^ν with the given neutrino flux Φ^ν gives the expected number of neutrinos either from a signal source or from background. We optimize the signal to background ratio as presented below.

3. Signal simulation and results

In this Section we describe the results of the numerical simulation of the neutrino signal from dark matter annihilations in the Sun. For the calculations we use a numerical procedure which has been described in Ref. [25]. Here we only briefly sketch the main ingredients of these simulations.

In any particular model the neutrino signal from dark matter annihilations in the Sun depends on combinations of different annihilation channels. For a model-independent approach we suppose that dark matter annihilates over particular channels with 100% branching ratio and give separate limits for each case. As representative annihilation channels we have chosen the conventional $b\bar{b}$, $\tau^+\tau^-$, W^+W^- decays and in addition the direct annihilation into neutrinos $\nu_e\bar{\nu}_e$, $\nu_\mu\bar{\nu}_\mu$ and $\nu_\tau\bar{\nu}_\tau$. The latter annihilation channels yield the most energetic neutrinos. The neutrino spectra at the production point have been calculated using the WimpSIM package [30, 31] which uses PYTHIA for this purpose. Subsequently we propagate neutrinos from the Sun to the Earth, taking into account neutrino oscillations in vacuum and in the media of the Sun and the Earth, and NC and CC neutrino interactions of neutrinos with nucleons. We use the solar model presented in Ref. [33]. As neutrino oscillation parameters we use $\Delta m_{21}^2 = 7.62 \cdot 10^{-5} \text{ eV}^2$, $\Delta m_{31}^2 = 2.55 \cdot 10^{-3} \text{ eV}^2$, $\delta_{CP} = 0$, $\sin^2 \theta_{12} = 0.32$, $\sin^2 \theta_{23} = 0.49$, $\sin^2 \theta_{13} = 0.026$ which are suggested by current experimental results [32]. Also we take into account ν_τ regeneration. The results of these simulations are energy spectra $\frac{dN_{\nu\mu}}{dE_{\nu\mu}}$ for muon neutrinos and antineutrinos at the telescope location for different annihilation channels and values of the mass of dark matter particles. Using the neutrino energy spectra we simulate CC neutrino interactions in the media surrounding the telescope and propagate the muons in rock and water. We refer the reader to Ref. [25] for more details. We note in passing that in Ref. [51] a more thorough calculation of initial and final neutrino spectra has been performed which includes electroweak corrections to the spectra. We do not take them into account because we are going to present the comparison with the limits obtained by other experiments which did not take them into account either.

The Sun has an apparent size of about 0.5° and can be considered as a local point source. However, the expected muon signal has a much larger angular spread because of the kinematics of the initial CC neutrino interaction and because of the intrinsic angular resolution Ψ of the telescope. This rises the question about how to define the size of the cone half-angle around the direction towards the Sun in which the events will be counted. We optimize the values of this angle to obtain the tightest expected upper limits on the neutrino flux. For the optimization of the search cone sizes we follow the MRF approach [29]. For a given mass of the dark matter particle and for each annihilation channel we construct the expected limit on the neutrino flux $\Phi_{\nu+\bar{\nu}}^{exp}$ as a function of the cone half-angle ψ as follows

$$\Phi_{\nu+\bar{\nu}}^{exp}(\psi) = \frac{\bar{N}_S^{90}(\psi)}{A_{eff}(\psi) \times T}. \quad (3)$$

Here \bar{N}_S^{90} is the 90% C.L. upper limit on the number of neutrino events inside the given cone averaged over the number of signal events with a Poisson distribution, T is the livetime. The effective area $A_{eff}(\psi)$ is defined for a given angular window ψ and the muon neutrino energy spectrum $\frac{dN_{\nu\mu}}{dE_{\nu\mu}}$ at the telescope location as

$$A_{eff}(\psi) = \frac{\sum_{\nu_\mu, \bar{\nu}_\mu} \int_{E_{th}}^{m_{DM}} dE_{\nu\mu} A(E_{\nu\mu}, E_{th}) P(E_{\nu\mu}, \psi) \frac{dN_{\nu\mu}(E_{\nu\mu})}{dE_{\nu\mu}}}{\sum_{\nu_\mu, \bar{\nu}_\mu} \int_{E_{th}}^{m_{DM}} dE_{\nu\mu} P(E_{\nu\mu}, \psi) \frac{dN_{\nu\mu}(E_{\nu\mu})}{dE_{\nu\mu}}}. \quad (4)$$

Here $A(E_{\nu\mu}, E_{th})$ is defined according to (2) and the sum over muon neutrino and antineutrino is implied. The probability $P(E_{\nu\mu}, \psi)$ for neutrinos with energy $E_{\nu\mu}$ to produce a muon which falls within the cone of half-angular size ψ from the initial neutrino direction has been obtained as described above, taking into account the angular resolution of the telescope obtained from MC simulation of the detector response [20]. By minimizing the function (3) we find the optimal values of the half-cone angle. The corresponding effective

areas for different annihilation channels are shown in Fig. 3. As expected, $\nu\bar{\nu}$ annihilation channels lead to the largest effective areas and the soft $b\bar{b}$ annihilation channels to the smallest ones. The upper limit on the neutrino flux is obtained by Eq. (3) replacing \bar{N}_S^{90} with values of the actual upper limit N_S^{90} discussed in the previous section. The upper limits on the muon neutrino flux for all chosen annihilation channels, recalculated for a neutrino energy threshold of 1 GeV, are shown in Fig. 4 and listed in Table 1, for DM masses ranging from 30 GeV to 10 TeV. One can see that the direct neutrino channels result in the tightest limits. The limits for the $b\bar{b}$, $\tau^+\tau^-$ and W^+W^- channels are shown in Fig. 5 as limits on the muon flux and compared to results from other experiments.

The upper limits on the muon neutrino flux can be related to the upper limits on other physical quantities related to dark matter physics. First of all, the muon neutrino flux directly depends on the DM annihilation rate Γ_A in the Sun as follows

$$\Phi_{\nu_\mu} = \frac{\Gamma_A}{4\pi R^2} \sum_{\nu_\mu, \bar{\nu}_\mu} \int_{E_{th}}^{m_{DM}} dE_{\nu_\mu} \frac{dN_{\nu_\mu}}{dE_{\nu_\mu}}, \quad (5)$$

where R is the distance to the Sun, and $E_{th} = 10$ GeV is the threshold neutrino energy of NT200. The upper limits on the annihilation rate Γ_A for several values of dark matter particle masses and different annihilation channels is also presented in Table 1.

After the long-time evolution of the solar system the processes of capture and annihilation of dark matter in the Sun can reach an equilibrium. In this case the capture rate should be twice the annihilation rate and the upper limit on Γ_A can be recalculated to limits on the spin-dependent (SD, σ_{SD}^{UppLim}) and spin-independent (SI, σ_{SI}^{UppLim}) parts of the cross section of elastic scattering of dark matter on proton [35, 36] as follows

$$\sigma_{\chi,p}^{UppLim,SD}(m_\chi) = \lambda^{SD}(m_\chi) \cdot \Gamma_A^{UppLim}(m_\chi) \quad (6)$$

$$\sigma_{\chi,p}^{UppLim,SI}(m_\chi) = \lambda^{SI}(m_\chi) \cdot \Gamma_A^{UppLim}(m_\chi). \quad (7)$$

For completeness we present formulas for the coefficients λ^{SD} and λ^{SI} in appendix A, as described in Refs. [25]. Their values are obtained assuming $\rho_{DM} = 0.3$ GeV/cm³ for the local dark matter density and $v_d = 270$ km/s for the root-mean-square of the dark matter velocity dispersion.

Now let us discuss the systematic uncertainties of the obtained results. The experimental uncertainty is estimated to be 30% which includes uncertainties in the optical properties of water and of the sensitivity of the OMs (see details for example in Refs. [11], [37]). Among the main theoretical uncertainties we mention those related to neutrino properties (interactions and oscillations). We estimate the uncertainties due to present errors in oscillation parameters as about 8% for leptonic annihilation channels and 5% for W^+W^- and $b\bar{b}$. The errors in neutrino-nucleon cross sections results in uncertainties from 8% to 4% for dark matter masses ranging from 30 GeV to 10 TeV. The estimation has been done by varying neutrino oscillation parameters [32] or neutrino-nucleon cross section [39] within their known ranges of uncertainty. Other systematic uncertainties include nuclear formfactors, the solar chemical composition, the influence of planets on dark matter capture by the solar system as well as the dark matter velocity distribution [35, 42, 43]. Let us mention that some recent studies indicate a larger value for the local dark matter density around 0.4 GeV/cm³ [44] which would make the upper limits even stronger.

The incorporation of all systematic uncertainties for signal and background into the final upper limits have been performed by the standard way [40] and the using TRolke class in ROOT. A full description of the method can be found in [41], while for the extraction of the confidence intervals a likelihood function is used. Systematic uncertainties result in a degradation of the upper limits by 7-12%. The final results for half-cone angles γ , upper 90% limits on the number of signal events N_S^{90} , the muon flux Φ_μ , the dark matter annihilation rate in the Sun Γ_A , the dark matter -proton spin-dependent $\sigma_{\chi p}^{SD}$ and spin-independent $\sigma_{\chi p}^{SI}$ scattering cross sections and neutrino fluxes Φ_ν are shown in Table 1. The fluxes have been recalculated to an energy threshold of 1 GeV. In Fig. 6 we present the Baikal upper limits on SD cross section for the annihilation channels $b\bar{b}$, W^+W^- and $\tau^+\tau^-$ (red lines) in comparison with the results of indirect searches by the ANTARES [26], Baksan [25], IceCube [28] (where ‘‘hard’’ means either $\tau^+\tau^-$ or W^+W^- channel correspondingly to DM masses which could be lighter or heavier than W-boson) and Super-Kamionande [27]

$m_{\text{DM}}, \text{GeV}$	channel	γ, deg	N_s^{90}	$\Phi_\mu, \text{km}^{-2}/\text{yr}$	Γ_A, s^{-1}	$\sigma_{\chi p}^{SI}, \text{pb}$	$\sigma_{\chi p}^{SD}, \text{pb}$	$\Phi_{\nu_\mu}, \text{km}^{-2}/\text{yr}$
30.0	bb	10.6	1.2	$6.6 \cdot 10^5$	$1.4 \cdot 10^{27}$	$8.2 \cdot 10^{-3}$	1.3	$3.8 \cdot 10^{16}$
	$\tau^+\tau^-$	9.2	0.57	$2.3 \cdot 10^4$	$2.3 \cdot 10^{23}$	$1.4 \cdot 10^{-5}$	$2.3 \cdot 10^{-3}$	$2.3 \cdot 10^{14}$
	$\nu_e\bar{\nu}_e$	9.3	0.50	$9.2 \cdot 10^3$	$2.4 \cdot 10^{23}$	$1.4 \cdot 10^{-6}$	$2.4 \cdot 10^{-4}$	$1.5 \cdot 10^{13}$
	$\nu_\mu\bar{\nu}_\mu$	8.5	1.1	$1.2 \cdot 10^4$	$2.9 \cdot 10^{23}$	$1.7 \cdot 10^{-6}$	$2.8 \cdot 10^{-4}$	$2.1 \cdot 10^{13}$
	$\nu_\tau\bar{\nu}_\tau$	8.1	1.3	$2.3 \cdot 10^4$	$5.7 \cdot 10^{23}$	$3.4 \cdot 10^{-6}$	$5.6 \cdot 10^{-4}$	$4.2 \cdot 10^{13}$
50.0	bb	9.4	0.43	$3.3 \cdot 10^4$	$2.8 \cdot 10^{25}$	$2.5 \cdot 10^{-4}$	$6.3 \cdot 10^{-2}$	$8.3 \cdot 10^{14}$
	$\tau^+\tau^-$	8.2	1.3	$1.5 \cdot 10^4$	$5.7 \cdot 10^{23}$	$5.2 \cdot 10^{-6}$	$1.3 \cdot 10^{-3}$	$5.6 \cdot 10^{13}$
	$\nu_e\bar{\nu}_e$	8.1	1.3	$9.9 \cdot 10^3$	$1.1 \cdot 10^{23}$	$1.0 \cdot 10^{-6}$	$2.6 \cdot 10^{-4}$	$6.2 \cdot 10^{12}$
	$\nu_\mu\bar{\nu}_\mu$	7.5	1.7	$8.1 \cdot 10^3$	$7.7 \cdot 10^{22}$	$7.0 \cdot 10^{-7}$	$1.8 \cdot 10^{-4}$	$5.5 \cdot 10^{12}$
	$\nu_\tau\bar{\nu}_\tau$	7.5	1.7	$8.2 \cdot 10^3$	$7.8 \cdot 10^{22}$	$6.9 \cdot 10^{-7}$	$1.7 \cdot 10^{-4}$	$5.4 \cdot 10^{12}$
100.0	bb	8.2	1.3	$2.1 \cdot 10^4$	$5.5 \cdot 10^{24}$	$1.0 \cdot 10^{-4}$	$4.5 \cdot 10^{-2}$	$1.7 \cdot 10^{14}$
	$\tau^+\tau^-$	7.2	1.9	$7.8 \cdot 10^3$	$8.7 \cdot 10^{22}$	$1.6 \cdot 10^{-6}$	$7.1 \cdot 10^{-4}$	$8.3 \cdot 10^{12}$
	W^+W^-	7.2	1.9	$7.9 \cdot 10^3$	$2.1 \cdot 10^{23}$	$4.0 \cdot 10^{-6}$	$1.7 \cdot 10^{-3}$	$7.2 \cdot 10^{12}$
	$\nu_e\bar{\nu}_e$	7.1	2.0	$7.7 \cdot 10^3$	$2.7 \cdot 10^{22}$	$5.0 \cdot 10^{-7}$	$2.2 \cdot 10^{-4}$	$1.3 \cdot 10^{12}$
	$\nu_\mu\bar{\nu}_\mu$	6.6	2.3	$4.7 \cdot 10^3$	$1.4 \cdot 10^{22}$	$2.6 \cdot 10^{-7}$	$1.1 \cdot 10^{-4}$	$9.4 \cdot 10^{11}$
	$\nu_\tau\bar{\nu}_\tau$	6.6	2.3	$4.5 \cdot 10^3$	$1.2 \cdot 10^{22}$	$2.8 \cdot 10^{-7}$	$1.2 \cdot 10^{-4}$	$9.7 \cdot 10^{11}$
200.0	bb	7.4	1.8	$1.1 \cdot 10^4$	$1.1 \cdot 10^{24}$	$5.0 \cdot 10^{-5}$	$3.4 \cdot 10^{-2}$	$3.6 \cdot 10^{13}$
	$\tau^+\tau^-$	6.4	2.4	$4.5 \cdot 10^3$	$1.7 \cdot 10^{22}$	$7.7 \cdot 10^{-7}$	$5.3 \cdot 10^{-4}$	$1.6 \cdot 10^{12}$
	W^+W^-	6.3	2.4	$3.9 \cdot 10^3$	$3.8 \cdot 10^{22}$	$1.3 \cdot 10^{-6}$	$1.4 \cdot 10^{-3}$	$2.1 \cdot 10^{11}$
	$\nu_e\bar{\nu}_e$	6.3	2.4	$4.5 \cdot 10^3$	$8.8 \cdot 10^{21}$	$3.9 \cdot 10^{-7}$	$2.8 \cdot 10^{-4}$	$2.7 \cdot 10^{11}$
	$\nu_\mu\bar{\nu}_\mu$	6.0	2.6	$2.5 \cdot 10^3$	$3.4 \cdot 10^{21}$	$1.5 \cdot 10^{-7}$	$1.0 \cdot 10^{-4}$	$1.9 \cdot 10^{11}$
	$\nu_\tau\bar{\nu}_\tau$	6.0	2.6	$2.6 \cdot 10^3$	$3.2 \cdot 10^{21}$	$1.5 \cdot 10^{-7}$	$9.9 \cdot 10^{-5}$	$2.2 \cdot 10^{11}$
500.0	bb	6.5	2.3	$5.9 \cdot 10^3$	$2.3 \cdot 10^{23}$	$4.1 \cdot 10^{-5}$	$4.2 \cdot 10^{-2}$	$7.4 \cdot 10^{12}$
	$\tau^+\tau^-$	5.7	2.7	$2.3 \cdot 10^3$	$2.9 \cdot 10^{21}$	$5.2 \cdot 10^{-7}$	$5.4 \cdot 10^{-4}$	$2.7 \cdot 10^{11}$
	W^+W^-	5.6	2.8	$1.2 \cdot 10^3$	$7.6 \cdot 10^{21}$	$1.3 \cdot 10^{-6}$	$1.4 \cdot 10^{-3}$	$2.1 \cdot 10^{11}$
	$\nu_e\bar{\nu}_e$	5.5	2.8	$1.1 \cdot 10^3$	$2.2 \cdot 10^{21}$	$3.8 \cdot 10^{-7}$	$4.0 \cdot 10^{-4}$	$2.3 \cdot 10^{10}$
	$\nu_\mu\bar{\nu}_\mu$	5.5	2.8	$1.0 \cdot 10^3$	$8.2 \cdot 10^{20}$	$1.5 \cdot 10^{-7}$	$1.5 \cdot 10^{-4}$	$2.2 \cdot 10^{10}$
	$\nu_\tau\bar{\nu}_\tau$	5.5	2.8	$1.4 \cdot 10^3$	$9.0 \cdot 10^{20}$	$1.6 \cdot 10^{-7}$	$1.7 \cdot 10^{-4}$	$7.2 \cdot 10^{10}$
1000.0	bb	6.1	2.5	$4.1 \cdot 10^3$	$9.5 \cdot 10^{22}$	$5.5 \cdot 10^{-5}$	$6.9 \cdot 10^{-2}$	$2.9 \cdot 10^{12}$
	$\tau^+\tau^-$	5.5	2.8	$1.4 \cdot 10^3$	$1.2 \cdot 10^{21}$	$6.8 \cdot 10^{-7}$	$8.4 \cdot 10^{-4}$	$1.1 \cdot 10^{11}$
	W^+W^-	5.5	2.8	$1.2 \cdot 10^3$	$3.8 \cdot 10^{21}$	$2.2 \cdot 10^{-6}$	$2.7 \cdot 10^{-3}$	$9.8 \cdot 10^{10}$
	$\nu_e\bar{\nu}_e$	5.3	2.9	$6.7 \cdot 10^2$	$1.5 \cdot 10^{21}$	$8.6 \cdot 10^{-7}$	$1.1 \cdot 10^{-3}$	$8.1 \cdot 10^9$
	$\nu_\mu\bar{\nu}_\mu$	5.3	2.9	$5.2 \cdot 10^2$	$1.0 \cdot 10^{21}$	$6.0 \cdot 10^{-7}$	$7.5 \cdot 10^{-4}$	$9.4 \cdot 10^9$
	$\nu_\tau\bar{\nu}_\tau$	5.5	2.8	$1.1 \cdot 10^3$	$6.8 \cdot 10^{20}$	$4.0 \cdot 10^{-7}$	$5.0 \cdot 10^{-4}$	$5.8 \cdot 10^{10}$
2000.0	bb	5.8	2.7	$3.0 \cdot 10^3$	$7.4 \cdot 10^{20}$	$1.0 \cdot 10^{-4}$	0.14	$1.5 \cdot 10^{12}$
	$\tau^+\tau^-$	5.4	2.9	$1.2 \cdot 10^3$	$1.2 \cdot 10^{21}$	$1.6 \cdot 10^{-6}$	$2.1 \cdot 10^{-3}$	$7.5 \cdot 10^{10}$
	W^+W^-	5.4	2.9	$1.1 \cdot 10^3$	$3.2 \cdot 10^{21}$	$6.8 \cdot 10^{-6}$	$9.2 \cdot 10^{-3}$	$8.0 \cdot 10^{10}$
	$\nu_e\bar{\nu}_e$	5.3	2.9	$7.5 \cdot 10^2$	$5.8 \cdot 10^{21}$	$1.2 \cdot 10^{-5}$	$1.7 \cdot 10^{-2}$	$1.4 \cdot 10^{10}$
	$\nu_\mu\bar{\nu}_\mu$	5.3	2.9	$6.9 \cdot 10^2$	$3.7 \cdot 10^{21}$	$7.9 \cdot 10^{-6}$	$1.1 \cdot 10^{-2}$	$1.5 \cdot 10^{10}$
	$\nu_\tau\bar{\nu}_\tau$	5.4	2.9	$1.1 \cdot 10^3$	$6.4 \cdot 10^{20}$	$1.3 \cdot 10^{-6}$	$1.9 \cdot 10^{-3}$	$5.8 \cdot 10^{10}$
5000.0	bb	5.6	2.8	$2.4 \cdot 10^3$	$2.9 \cdot 10^{22}$	$3.7 \cdot 10^{-4}$	0.53	$8.2 \cdot 10^{11}$
	$\tau^+\tau^-$	5.4	2.9	$1.1 \cdot 10^3$	$5.9 \cdot 10^{20}$	$7.5 \cdot 10^{-6}$	$1.1 \cdot 10^{-2}$	$6.3 \cdot 10^{10}$
	W^+W^-	5.4	2.9	$1.1 \cdot 10^3$	$2.9 \cdot 10^{21}$	$3.6 \cdot 10^{-5}$	$5.3 \cdot 10^{-2}$	$7.1 \cdot 10^{10}$
	$\nu_e\bar{\nu}_e$	5.3	2.9	$9.5 \cdot 10^2$	$2.1 \cdot 10^{22}$	$2.7 \cdot 10^{-4}$	$3.8 \cdot 10^{-1}$	$2.1 \cdot 10^{10}$
	$\nu_\mu\bar{\nu}_\mu$	5.6	2.8	$7.1 \cdot 10^2$	$1.1 \cdot 10^{22}$	$1.4 \cdot 10^{-4}$	$2.1 \cdot 10^{-1}$	$2.1 \cdot 10^{10}$
	$\nu_\tau\bar{\nu}_\tau$	5.3	2.9	$1.1 \cdot 10^3$	$5.9 \cdot 10^{20}$	$7.4 \cdot 10^{-6}$	$1.1 \cdot 10^{-2}$	$5.4 \cdot 10^{10}$
10000.0	bb	5.7	2.7	$1.9 \cdot 10^3$	$2.2 \cdot 10^{22}$	$1.1 \cdot 10^{-3}$	1.58	$5.4 \cdot 10^{11}$
	$\tau^+\tau^-$	5.4	2.9	$1.2 \cdot 10^3$	$5.4 \cdot 10^{20}$	$2.7 \cdot 10^{-5}$	$3.9 \cdot 10^{-2}$	$5.9 \cdot 10^{10}$
	W^+W^-	5.4	2.9	$1.0 \cdot 10^3$	$2.7 \cdot 10^{21}$	$1.3 \cdot 10^{-4}$	0.19	$6.5 \cdot 10^{10}$
	$\nu_e\bar{\nu}_e$	5.3	2.8	$8.8 \cdot 10^2$	$4.1 \cdot 10^{22}$	$2.0 \cdot 10^{-3}$	2.96	$2.0 \cdot 10^{10}$
	$\nu_\mu\bar{\nu}_\mu$	5.3	2.9	$7.7 \cdot 10^2$	$2.5 \cdot 10^{22}$	$1.3 \cdot 10^{-3}$	1.8	$2.3 \cdot 10^{10}$
	$\nu_\tau\bar{\nu}_\tau$	5.4	2.9	$1.0 \cdot 10^3$	$5.4 \cdot 10^{20}$	$2.7 \cdot 10^{-5}$	$3.9 \cdot 10^{-2}$	$5.0 \cdot 10^{10}$

Table 1: Half-cone angles γ , 90% upper limits N_S^{90} on the number of signal events, the muon flux Φ_μ , the dark matter annihilation rate in the Sun Γ_A , the dark matter-proton spin-dependent $\sigma_{\chi p}^{SD}$ and spin-independent $\sigma_{\chi p}^{SI}$ scattering cross sections and neutrino fluxes Φ_ν .

collaborations. Obviously, each experiment has better sensitivity for harder neutrino spectra from $\tau^+\tau^-$ annihilation channel. In Fig. 7 we compare the Baikal upper limits for all six chosen annihilation channels including annihilations into monochromatic neutrinos with the results of direct searches by PICASSO [45], KIMS [46], SIMPLE [47], DAMA [48, 49] and COUPP [50]. Obviously, the neutrino telescope bounds are complementary to direct detection results. The upper limits on SD and SI cross sections obtained with NT200 results refer to 100% branching ratio of the corresponding annihilation channels. In general model one expects that these upper bounds lie somewhere between those annihilation channels for the softest and hardest neutrino spectra if DM particles annihilate over them with a considerable fraction. Otherwise the limits are weakened by corresponding branching ratio. This should be beared in mind when comparing them with the results of direct searches. Let us comment at this point about the behaviour of the upper limits for direct neutrino annihilation channels (pink lines). Clearly, these limits are considerably stronger than those for $b\bar{b}$, W^+W^- and $\tau^+\tau^-$ channels (red lines) for $m_{DM} \lesssim 700$ GeV. This is related to the fact that the neutrino spectrum at production in the Sun for $\nu\bar{\nu}$ channels is more energetic and a harder neutrino energy spectrum is expected at the telescope location. At the same time for larger masses $m_{DM} \gtrsim 700$ GeV a suppression in the upper limits arises because of increasing CC and NC neutrino-nucleon cross sections which result in considerable absorption of ν_e and ν_μ and their antineutrinos in the Sun. However, because of the effect of ν_τ regeneration, the corresponding neutrinos reappear after CC interactions with somewhat lower energy. Therefore the limits for $\tau^+\tau^-$ and $\nu_\tau\bar{\nu}_\tau$ annihilations channels are quite similar for very large DM masses. These observations indicate that indirect searches with neutrino telescopes are more sensitive to leptophilic dark matter models than to others.

4. Conclusions

To summarize, we have studied the NT200 response to neutrinos from dark matter annihilations in the Sun. We have derived upper limits on the muon and neutrino fluxes, the annihilation rate and on the SD/SI cross sections of DM scattering on protons assuming different annihilation channels. We have found that for DM masses below 500 GeV the best sensitivity is obtained for the annihilation in neutrino-antineutrino pairs. For heavier dark matter particles the most stringent limits are obtained for leptonic $\tau^+\tau^-$ and ν_τ annihilation channels.

Acknowledgments

We are grateful to C. Spiering for valuable comments. The research was supported in part by RFBR grant 13-02-12221, by RFBR grant 14-02-00972, by RFBR grant 13-02-01127 (S.D.) and by grant of the President of the Russian Federation NS-2835.2014.2 (S.D.).

References

- [1] Spergel, D. N., Verde, L., Peiris, H. V. et al., “First Year Wilkinson Microwave Anisotropy Probe (WMAP) Observations: Determination of Cosmological Parameters,” *ApJS*, 148, 175, 2003, arXiv:astro-ph/0302209.
- [2] Hinshaw, G., Larson, D., Komatsu, E., et al., “Nine-Year Wilkinson Microwave Anisotropy Probe (WMAP) Observations: Cosmological Parameter Results,” 2012, arXiv:1212.5226.
- [3] Planck collaboration, P. A. R. Ade et al., “Planck 2013 results. XV. CMB power spectra and likelihood,” 2013, arXiv:1303.5075.
- [4] Reichardt, C. L., Shaw, L., Zahn, O., et al., “A measurement of secondary cosmic microwave background anisotropies with two years of South Pole Telescope observations,” *ApJ*, 755, 70, 2012, arXiv:1111.0932.
- [5] D. Clowe et al., “On dark peaks and missing mass: a weak-lensing mass reconstruction of the merging cluster system A520,” *ApJ* 758, p 128, 2012.
- [6] G. Jungman, M. Kamionkowski and K. Griest, “Supersymmetric dark matter,” *Phys. Rept.* **267** (1996) 195 [hep-ph/9506380].
- [7] D. Hooper and S. Profumo, “Dark matter and collider phenomenology of universal extra dimensions,” *Phys. Rept.* **453** (2007) 29 [hep-ph/0701197].

- [8] K. M. Belotsky, M. Y. Khlopov and K. I. Shibaev, “Monochromatic neutrinos from massive fourth generation neutrino annihilation in the sun and earth,” *Part. Nucl. Lett.* **108** (2001) 5. K. M. Belotsky, T. Damour and M. Y. Khlopov, “Implications of a solar system population of massive fourth generation neutrinos for underground searches of monochromatic neutrino annihilation signals,” *Phys. Lett. B* **529** (2002) 10 [astro-ph/0201314]. K. Belotsky, M. Khlopov and C. Kouvaris, “Muon flux limits for Majorana dark matter from strong coupling theories,” *Phys. Rev. D* **79** (2009) 083520 [arXiv:0810.2022 [astro-ph]].
- [9] K. Griest and D. Seckel, “Cosmic Asymmetry, Neutrinos and the Sun,” *Nucl. Phys. B* **283** (1987) 681 [Erratum-ibid. B **296** (1988) 1034].
- [10] U.F. Katz, Ch. Spiering, “High-energy neutrino astrophysics: Status and perspectives.,” *Progress in Particle and Nuclear Physics*, vol. 67, issue 3, p. 651-704, 2012.
- [11] A. V. Avrorin et al., “Search for astrophysical neutrinos in the Baikal neutrino project,” *Phys. Part. Nucl. Lett.* vol. 8, 704, 2011.
- [12] A. V. Avrorin et al., “Current status of the BAIKAL-GVD project,” *Nucl. Instrum. Meth.* A725, p 23, 2013.
- [13] A. V. Avrorin et al., “Search for Neutrinos from Dark Matter Annihilation in the Sun with the Baikal Neutrino Experiment,” *Proc. of the 31st ICRC, Lodz, Poland*, 2009.
- [14] Y. Farzan, “Flavoring Monochromatic Neutrino Flux from Dark Matter Annihilation,” *JHEP* **1202** (2012) 091, [arXiv:1111.1063 [hep-ph]].
- [15] A. Esmaili and Y. Farzan, “A Novel Method to Extract Dark Matter Parameters from Neutrino Telescope Data,” *JCAP* **1104** (2011) 007, [arXiv:1011.0500 [hep-ph]].
- [16] L. Bergstrom, “Dark Matter Evidence, Particle Physics Candidates and Detection Methods”, *Annalen Phys.* 524 (2012) 479-496, arXiv:1205.4882 [astro-ph.HE]
- [17] V. Aynutdinov et al., “The Baikal Neutrino experiment: Status, selected physics results, and perspectives,” *Izvestia Akademii Nauk (Izvestia Russ. Academy Science), Ser. Phys.*, vol. 71, N. 4, 2007.
- [18] V. Aynutdinov et al., “The BAIKAL neutrino experiment: Physics results and perspectives,” *Nucl. Instrum. Methods*, vol A602, p 14, 2009.
- [19] A. D. Avrorin et al., “Status and recent results of the BAIKAL-GVD project”, is to appear in *Physics of Particles and Nuclei*, JINR, Dubna, to be published in 2015.
- [20] I. A. Belolaptikov, Preprint of INR RAS 1178/2007 (in Russian), 2007
- [21] V. Agrawal, T. Gaissler, P. Lipari and T. Stanev, “Atmospheric neutrino flux above 1 GeV,” *Phys. Rev.*, vol. D53, p. 1314, 1996.
- [22] D. Heck et al., Forschungszentrum Karlsruhe, Technical Report No. 6019, 1998.
- [23] E. Bugaev, S. Klimushin, I. Sokalsky, *Phys. Rev. D*, vol. 64, p. 074015, 2001.
- [24] <http://root.cern.ch> R. Brun et al., *Nucl. Instrum. Methods in Phys. Res.*, 1996
- [25] M. M. Boliev, S. V. Demidov, S. P. Mikheyev and O. V. Suvorova, “Search for muon signal from dark matter annihilations in the Sun with the Baksan Underground Scintillator Telescope for 24.12 years,” *JCAP* **1309** (2013) 019 [arXiv:1301.1138 [astro-ph.HE]].
- [26] S. Adrian-Martinez *et al.* [ANTARES Collaboration], “First results on dark matter annihilation in the Sun using the ANTARES neutrino telescope,” *JCAP* **1311** (2013) 032 [arXiv:1302.6516 [astro-ph.HE]].
- [27] T. Tanaka *et al.* [Super-Kamiokande Collaboration], “An Indirect Search for WIMPs in the Sun using 3109.6 days of upward-going muons in Super-Kamiokande”, *Astrophys. J.* **742**, 78, (2011)[arXiv:1108.3384 [astro-ph.HE]].
- [28] M. G. Aartsen *et al.* [IceCube Collaboration], “Search for dark matter annihilations in the Sun with the 79-string IceCube detector,” *Phys. Rev. Lett.* **110**, 131302, (2013) [arXiv:1212.4097 [astro-ph.HE]].
- [29] G. C. Hill and K. Rawlins, “Unbiased cut selection for optimal upper limits in neutrino detectors: The Model rejection potential technique,” *Astropart. Phys.* **19** (2003) 393 [astro-ph/0209350].
- [30] J. Edsjo, WimpSim Neutrino Monte Carlo, <http://www.fysik.su.se/~edsjo/wimpsim/>
- [31] M. Blennow, J. Edsjo and T. Ohlsson, “Neutrinos from WIMP annihilations using a full three-flavor Monte Carlo,” *JCAP* **0801** (2008) 021 [arXiv:0709.3898 [hep-ph]].
- [32] D. V. Forero, M. Tortola and J. W. F. Valle, “Global status of neutrino oscillation parameters after Neutrino-2012,” *Phys. Rev. D* **86** (2012) 073012 [arXiv:1205.4018 [hep-ph]].
- [33] J. N. Bahcall, A. M. Serenelli and S. Basu, “New solar opacities, abundances, helioseismology, and neutrino fluxes,” *Astrophys. J.* **621** (2005) L85 [astro-ph/0412440].
- [34] N. Grevesse and A. J. Sauval, “Standard Solar Composition,” *Space Sci. Rev.* **85** (1998) 161.
- [35] G. Wikstrom and J. Edsjo, “Limits on the WIMP-nucleon scattering cross-section from neutrino telescopes,” *JCAP* **0904** (2009) 009 [arXiv:0903.2986 [astro-ph.CO]].
- [36] S. Demidov and O. Suvorova, “Annihilation of NMSSM neutralinos in the Sun and neutrino telescope limits,” *JCAP* **1006** (2010) 018 [arXiv:1006.0872 [hep-ph]].
- [37] K. Antipin et al., “Search for relativistic magnetic monopoles with the Baikal Neutrino Telescope,” BAIKAL Collaboration (K. Antipin (Moscow, INR) et al.). Jan 2007. 5 pp. Published in *Astropart. Phys.* 29 (2008) 366-372 DOI: 10.1016/j.astropartphys.2008.03.006
- [38] A. Gould, “Cosmological density of WIMPs from solar and terrestrial annihilations,” *Astrophys. J.* 388 (1992) 338. A. Gould, “Resonant Enhancements In Wimp Capture By The Earth,” *Astrophys. J.* 321 (1987) 571.
- [39] A. Cooper-Sarkar, P. Mertsch and S. Sarkar, “The high energy neutrino cross-section in the Standard Model and its uncertainty,” *JHEP* **1108** (2011) 042 [arXiv:1106.3723 [hep-ph]].
- [40] J. Beringer *et al.* [Particle Data Group Collaboration], “Review of Particle Physics (RPP),” *Phys. Rev. D* **86** (2012) 010001.

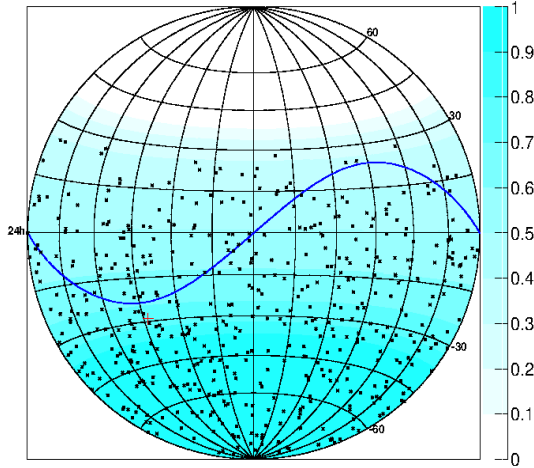


Figure 1: Skymap with NT200 neutrino events in equatorial coordinates. The blue curve marks the path of the Sun, the red cross – the location of the Galactic Center.

- [41] Wolfgang A. Rolke, Angel M. Lopez, Jan Conrad, “Limits and confidence intervals in the presence of nuisance parameters,” *Nucl.Instrum.Meth.* **A551** (2005) 493-503
- [42] C. Rott, T. Tanaka and Y. Itow, “Enhanced Sensitivity to Dark Matter Self-annihilations in the Sun using Neutrino Spectral Information,” *JCAP* **1109** (2011) 029 [arXiv:1107.3182 [astro-ph.HE]].
- [43] K. Choi, C. Rott, and Y. Itow, “Impact of Dark Matter Velocity Distributions on Capture Rates in the Sun,” *JCAP* **1405** (2014) 049 [arXiv:1312.0273 [astro-ph.HE]].
- [44] R. Catena and P. Ullio, “A novel determination of the local dark matter density,” *JCAP* **1008** (2010) 004 [arXiv:0907.0018 [astro-ph.CO]].
- [45] S. Archambault *et al.* [PICASSO Collaboration], “Constraints on Low-Mass WIMP Interactions on ^{19}F from PICASSO,” *Phys. Lett. B* **711** (2012) 153 [arXiv:1202.1240 [hep-ex]].
- [46] S. C. Kim, H. Bhang, J. H. Choi, W. G. Kang, B. H. Kim, H. J. Kim, K. W. Kim and S. K. Kim *et al.*, “New Limits on Interactions between Weakly Interacting Massive Particles and Nucleons Obtained with CsI(Tl) Crystal Detectors,” *Phys. Rev. Lett.* **108** (2012) 181301 [arXiv:1204.2646 [astro-ph.CO]].
- [47] M. Felizardo, T. A. Girard, T. Morlat, A. C. Fernandes, A. R. Ramos, J. G. Marques, A. Kling and J. Puibasset *et al.*, “Final Analysis and Results of the Phase II SIMPLE Dark Matter Search,” *Phys. Rev. Lett.* **108** (2012) 201302 [arXiv:1106.3014 [astro-ph.CO]].
- [48] R. Bernabei *et al.*, [DAMA Collab.], “First results from DAMA/LIBRA and the combined results with DAMA/NaI”, *Eur. Phys. J. C* **56** (2008) 333 [arXiv:astro-ph/0804.2741].
- [49] C. Savage, G. Gelmini, P. Gondolo and K. Freese, “Compatibility of DAMA/LIBRA dark matter detection with other searches,” *JCAP* **0904** (2009) 010 [arXiv:0808.3607 [astro-ph]].
- [50] E. Behnke, J. Behnke, S. J. Brice, D. Broemmelsiek, J. I. Collar, P. S. Cooper, M. Crisler and C. E. Dahl *et al.*, “Improved Limits on Spin-Dependent WIMP-Proton Interactions from a Two Liter CF₃I Bubble Chamber,” *Phys. Rev. Lett.* **106** (2011) 021303 [arXiv:1008.3518 [astro-ph.CO]].
- [51] P. Baratella, M. Cirelli, A. Hektor, J. Pata, M. Piibeleht and A. Strumia, “PPPC 4 DM ν : A Poor Particle Physicist Cookbook for Neutrinos from DM annihilations in the Sun,” arXiv:1312.6408 [hep-ph].

Appendix A. Calculation of λ^{SD} and λ^{SI}

In this Appendix we present the procedure used to calculate the coefficients λ^{SD} and λ^{SI} entering Eqs. (6) and (7). They can be obtained from known expressions [38] (see also [35]) for dark matter capture rate C and the equilibrium condition. The capture rate can be represented in the form of the following integral

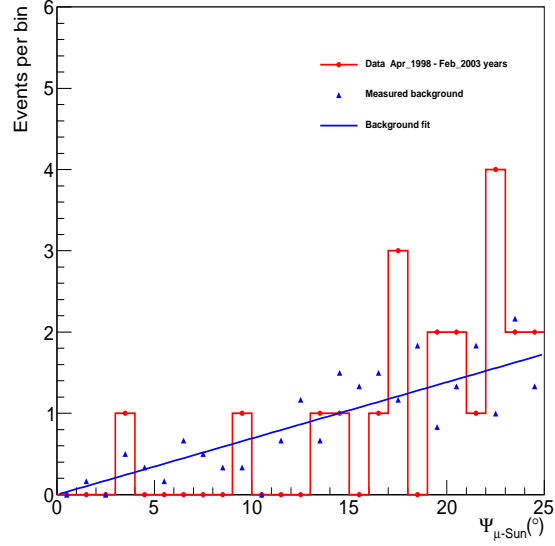


Figure 2: Data and background samples of mismatch angles to the Sun.

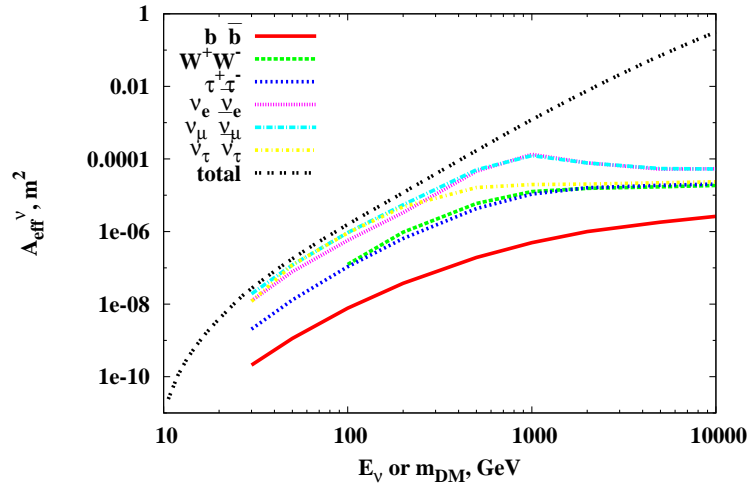


Figure 3: Effective area as a function of neutrino energy E_ν ("total") and as a function of the mass m_{DM} of the DM particle for different annihilation channels.

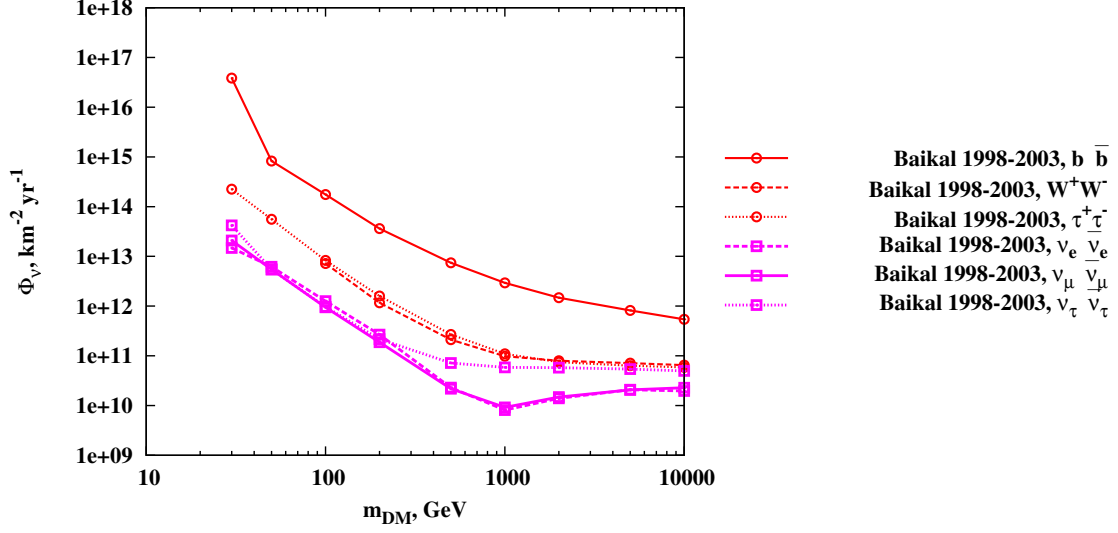


Figure 4: 90% CL upper limits on the muon neutrino flux for NT200.

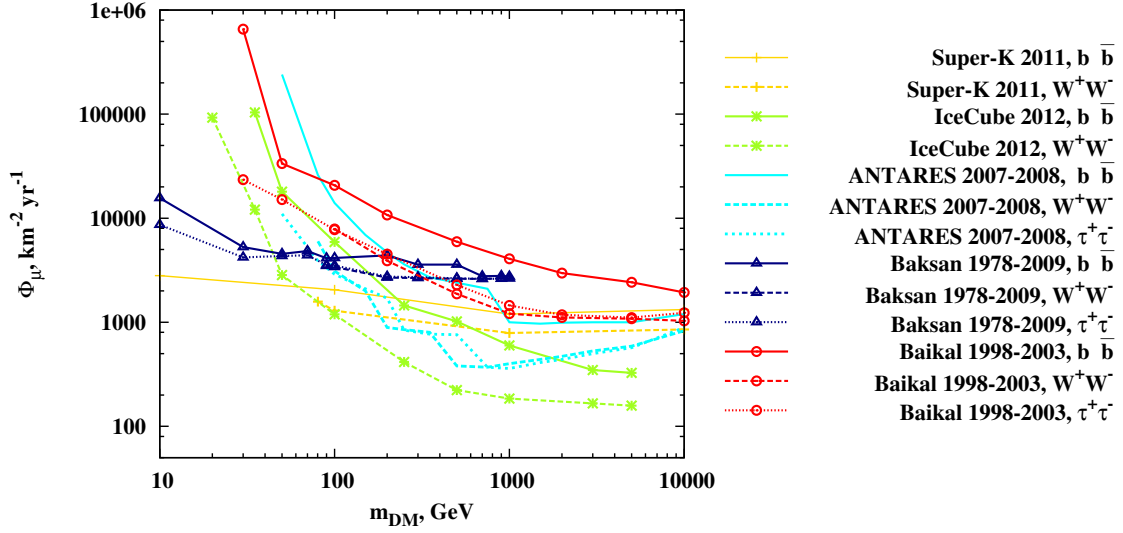


Figure 5: 90% CL upper limits on the muon flux for NT200 in comparison with the results from other neutrino telescopes.

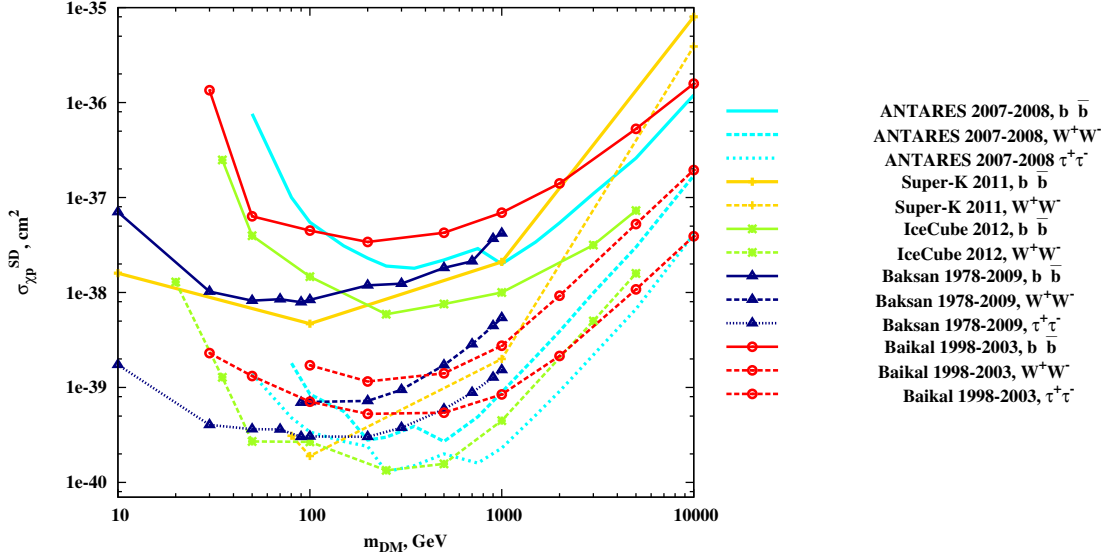


Figure 6: Comparison of Baikal 90% CL limits on the spin-dependent elastic cross section of DM particles on protons with the results of other indirect searches from ANTARES, Baksan, IceCube, SuperKamiokande.

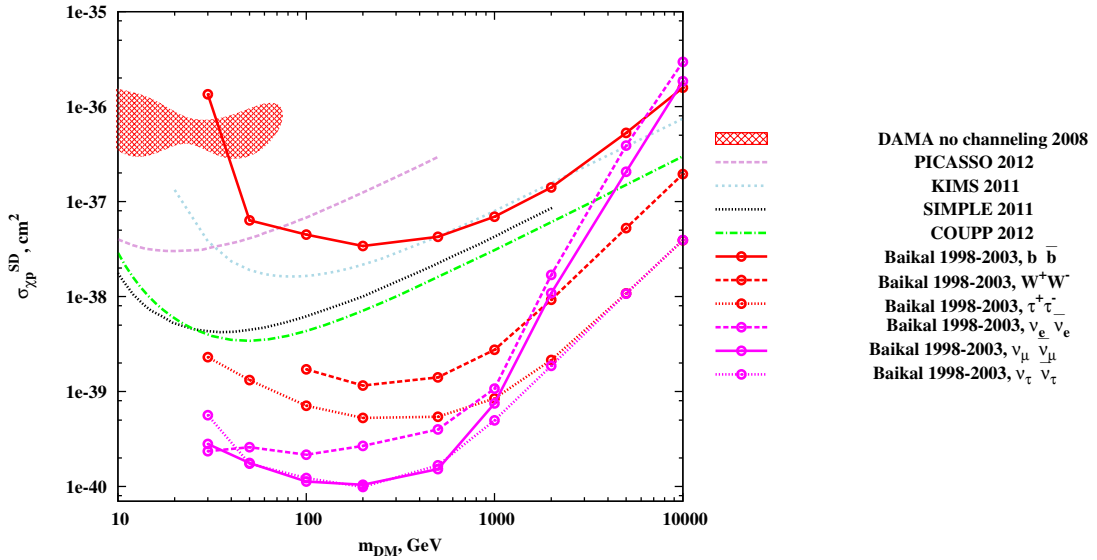


Figure 7: Comparison of Baikal 90% CL limits on the spin-dependent elastic cross section of DM particles on protons with the results of direct searches: DAMA, PICASSO, KIMS, SIMPLE, COUPP.

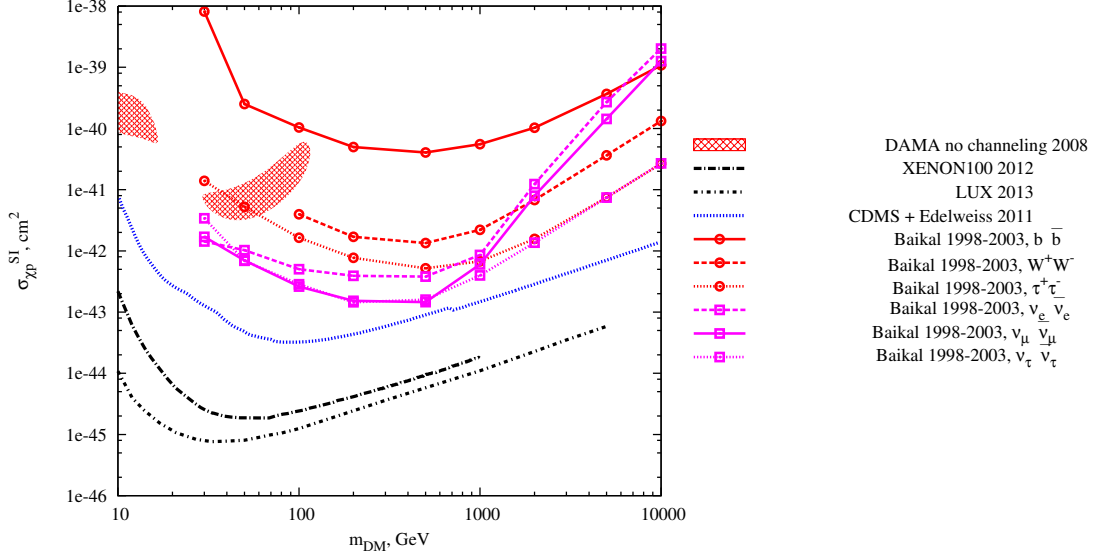


Figure 8: Comparison of Baikal 90% CL limits on the spin-independent elastic cross section of DM particles on protons with the results of direct searches: DAMA, CDMS/Edelweiss, XENON, LUX.

over the Sun volume

$$C = \int_0^{R_\odot} 4\pi r^2 dr \sum_i \frac{dC_i}{dV}, \quad (\text{A.1})$$

where R_\odot is the radius of the Sun and the sum goes over different types of nuclei in the Sun. The integrand in (A.1) is obtained by averaging of the capture probability over velocities u of dark matter particles as follows

$$\frac{dC_i}{dV} = \int_0^{u_{max}} du \frac{f(u)}{u} (w\Omega_{v,i}(w)). \quad (\text{A.2})$$

Here

$$u_{max} = 2v_{esc} \frac{\sqrt{\mu}}{\mu - 1}, \quad \mu = \frac{m_\chi}{m_i}, \quad w = \sqrt{u^2 + v_{esc}^2}, \quad (\text{A.3})$$

v_{esc} is escape velocity, m_i is the mass of i -th type of nuclei and the velocity distribution has the form

$$\frac{f(u)}{u} = \frac{3}{2\pi} \frac{\rho_\chi}{m_\chi v_d v_\odot} \left(\exp\left(-\frac{3(u - v_\odot)^2}{2v_d^2}\right) - \exp\left(-\frac{3(u + v_\odot)^2}{2v_d^2}\right) \right), \quad (\text{A.4})$$

where $v_d = 270$ km/s is velocity dispersion, $v_{Sun} = 220$ km/s is the velocity of the Sun relative to the dark matter halo, $\rho_\chi = 0.3$ GeV/cm³ is the local dark matter density. The capture probability per time unit and for i -th type of element $\Omega_{v,i}$ which enter Eq. (A.2) can be expressed as follows

$$w\Omega_{v,i}(w) = \sigma_{\chi,i} n_i \frac{(\mu + 1)^2}{2\mu} \frac{E_i^0}{m_\chi} \left[\exp\left(-\frac{m_\chi u^2}{2E_i^0}\right) - \exp\left(-\frac{2\mu}{(\mu + 1)^2} \frac{m_\chi w^2}{E_i^0}\right) \right], \quad (\text{A.5})$$

where $\sigma_{\chi,i}$ is the elastic cross section of the dark matter on the i -th type of nuclei, n_i is number density of the i -th element and the exponential suppression with a coherence energy

$$E_i^0 = \frac{3\hbar^2}{2m_\chi R_i^2}, \quad R_i = \left[0.91 \left(\frac{m_i}{\text{GeV}} \right)^{1/3} + 0.3 \right] \cdot 10^{-15} \text{ m} \quad (\text{A.6})$$

comes from a “form factor” in the cross section of dark matter particle on nuclei. For the SD part of the cross section σ^{SD} we take into account only scattering on hydrogen. As for the SI part of the cross section on the i -th type of nuclei it can be calculated as

$$\sigma_{\chi,i}^{SI} = \sigma^{SI} A_i^2 \frac{(m_\chi m_i)^2}{(m_\chi + m_i)^2} \frac{(m_\chi + m_p)^2}{(m_\chi m_p)^2} \quad (\text{A.7})$$

where σ^{SI} is the SI cross section of dark matter on proton, A_i is the atomic number and m_p is the proton mass. The expression for the capture rate can be divided into spin-dependent and spin-independent parts

$$C = C^{SD} + C^{SI} \quad (\text{A.8})$$

according to which type of cross section contributes to it. Finally, the coefficients entering (6) and (7) can be expressed as follows

$$\lambda^{SD}(m_\chi) = \frac{\sigma^{SD}}{2C^{SD}}, \quad \lambda^{SI}(m_\chi) = \frac{\sigma^{SI}}{2C^{SI}}, \quad (\text{A.9})$$

where the factor of 2 comes from the condition of equilibrium between capture and annihilation processes which implies $2C = \Gamma_A$. To obtain $\lambda^{SD}(m_\chi)$ and $\lambda^{SI}(m_\chi)$ we perform a numerical integration in Eqs. (A.1) and (A.2) using the solar model BS2005-OP of Ref. [33]. For elements heavier than oxygen the relative abundances were taken from Ref. [34].

Abstract

Keywords:

1.

References

Abstract

Keywords:

1.

References

[1]